Journal of Power Sources 256 (2014) 137–144

Contents lists available at ScienceDirect

Journal of Power Sources

journal homepage: www.elsevier.com/locate/jpowsour

A simple synthesis of hollow carbon nanofiber-sulfur composite via mixed-solvent process for lithium–sulfur batteries

Qiang Li [a], Zhian Zhang [a,b,*], Kai Zhang [a], Jing Fang [a], Yanqing Lai [a,b], Jie Li [a,b]

[a] School of Metallurgy and Environment, Central South University, Changsha, Hunan 410083, China
[b] Engineering Research Center of High Performance Battery Materials and Devices, Research Institute of Central South University in Shenzhen, Shenzhen 518057, China

HIGHLIGHTS

- HCNF-S composite prepared via a mixed-solvent process was applied for lithium–sulfur batteries.
- The prepared HCNF-S composite showed a highly conductive network-like structure.
- The HCNF-S composite showed perfect cycling stability and rate capability.
- The hollow fibrous HCNFs would be a promising carbon matrix for Li–S batteries.

ARTICLE INFO

Article history:
Received 19 October 2013
Received in revised form
21 December 2013
Accepted 13 January 2014
Available online 23 January 2014

Keywords:
Lithium–sulfur batteries
Hollow carbon nanofiber
Mixed-solvent process
Network-like structure
Polysulfides

ABSTRACT

A hollow carbon nanofiber supported sulfur (HCNF-S) composite cathode material is prepared by a mixed-solvent (DMF/CS_2) process in an organic solution for lithium–sulfur batteries. Scanning electron microscope (SEM) and transmission electron microscope (TEM) observations show the hollow structures of the HCNF and the homogeneous distribution of sulfur in the composite. The performance of the HCNF-S cathode is evaluated in lithium-sulfur batteries using cyclic voltammetry, galvanostatic charge–discharge, and electrochemical impedance spectroscopy. It is found that the HCNF-S cathode shows perfect cycling stability. The results exhibit an initial discharge capacity of 1090 mAh g^{-1} and retains 600 mAh g^{-1} after 100 discharge/charge cycles at a high rate of 1 C. The excellent electrochemical properties benefit from the hollow and highly conductive network-like structure of HCNFs, which contribute to disperse sulfur and absorb polysulfides, and suppress the formation of residual Li_2S layer.

1. Introduction

The lithium-sulfur (Li–S) system, based on the electrochemical reaction $16Li + S_8 \leftrightarrow 8Li_2S$, is one of the most promising candidates for high energy density applications especially in electric vehicles (EVs) and hybrid electric vehicles (HEVs), due to its low cost, environment friendliness, availability of resource materials, large theoretical specific capacity and energy of 1675 mAh g^{-1} and 2500 Wh kg^{-1}, respectively [1–4]. Despite these significant advantages, the application of Li–S batteries still suffers from several serious challenges such as the low electrochemical utilization of sulfur, poor cycling stability, and poor rate capability [5–9]. These problems could be attributed to the poor electrical conductivity of sulfur and its reduced products and the dissolution and shuttling effect of the intermediate products lithium polysulfides (Li_2S_n, $4 \leq n \leq 8$) in organic liquid electrolytes during cycling [10–12].

To overcome these problems, many attempts have been made, which focus on enhancing the electrical conductivity of the cathode and suppressing the loss of soluble polysulfide intermediates during cycling [13,14]. Various conductive porous carbons [15–20], conducting polymers [21,22] and graphenes [23,24] have been used as host materials for sulfur cathode in recent years to improve the electrochemical performance of Li–S batteries. These carbon-sulfur and polymer-sulfur composites improve electrical conductivity and trap some of the soluble polysulfides during cycling. Among these efforts, conductive matrixes with hollow structures, such as hollow carbon spheres [25,26], polyaniline nanotubes [27] and carbon nanotubes [19,28] are very attractive materials, because the hollow structure might have several advantages including high surface

* Corresponding author. School of Metallurgy and Environment, Central South University, Changsha, Hunan 410083, China. Tel./fax: +86 731 88830649.
E-mail address: zza75@163.com (Z. Zhang).

0378-7753/$ – see front matter © 2014 Elsevier B.V. All rights reserved.
http://dx.doi.org/10.1016/j.jpowsour.2014.01.063

area for efficient sulfur uptake and polysulfides containment, sufficient space to withstand volumetric expansion and short transport length for lithium ions.

The hollow carbon nanofibers (HCNFs) are an attractive carbon material for the sulfur electrode, because linear carbon materials can provide an effective conduction path of lithium ions and an ideal network-like structure that forms a stable structure for trapping polysulfides during the charge-discharge process [19,29]. In recent years, the reports about HCNFs acting as host materials of elemental sulfur are relatively rare. Cui et al. [30] has reported a hollow carbon nanofiber-encapsulated sulfur cathode for effective trapping of polysulfides and demonstrate experimentally high specific capacity and excellent electrochemical cycling of the cells. In their research, hollow carbon nanofiber arrays were fabricated using anodic aluminum oxide (AAO) templates through thermal carbonization of polystyrene. To prepare hollow carbon nanofiber-sulfur composite, 15 mg of carbon-coated AAO template was loaded into a small glass vial and 300 μl of 1% sulfur solution in toluene was dropped onto the template. After drying, the mixture was heated up to 155 °C and kept for 12 h to facilitate sulfur diffusion into the hollow nanofibers. The high aspect ratio of hollow carbon nanofibers reduces the random diffusion of polysulfides in the organic electrolyte, while the thin carbon wall allows fast transport of lithium ions. In addition, Cairns et al. [31] has also reported a sulfur-coated carbon nanofiber composite cathode material prepared by a chemical deposition method based the reaction between sodium polysulfide and formic acid. The composite material exhibits good electrochemical properties in rechargeable lithium-sulfur cells due to the chain-like electron transport network of carbon nanofibers.

However, these kinds of intertwined linear nanostructured carbon materials such as CNTs and CNFs are difficult to be dispersed. Ultrasonication in solvents is usually a primary step for producing homogeneous and relatively aggregate-free dispersions. The dispersant used needs to overcome the strong van der Waals force between CNTs to resist their agglomeration [32]. Ham et al. [33] has proved N,N-dimethylformamide (DMF) to be better than ethanol, water, acetone and methanol for making CNTs dispersions, which is also confirmed by Inam et al. [34].

In this work, we report a well-dispersed hollow carbon nanofiber-sulfur (HCNF-S) composite material prepared by a simple method via a mixed-solvent (DMF/CS_2) process for rechargeable Li–S batteries. In this method, N,N-Dimethylformamide (DMF) acts as a dispersant for HCNFs and carbon disulfide (CS_2) dissolves elemental sulfur. The prepared HCNF-S composite material shows good dispersity and an ideal network-like structure, which forms a stable structure for trapping polysulfides during the charge-discharge process. Electrochemical results exhibit an initial discharge capacity of 1090 mAh $g^{-1}$and retains 600 mAh g^{-1} after 100 cycles at a high rate of 1 C. The excellent electrochemical properties benefit from the hollow and highly conductive network-like structure of HCNFs with abundant pores, which contribute to disperse sulfur and absorb polysulfides, and suppress the formation of residual Li_2S layer.

2. Experimental

2.1. Materials preparation

First, in order to compare the dispersion effects of HCNFs in deionized water and DMF, we designed and conducted a sedimentation experiment. Firstly, 50 mg HCNFs was added into a vial filled with 20 ml deionized water and DMF, respectively. Then, the two vials were hand-mixed for 30 s and high power bath ultrasonicated for 2 h at 20 °C. Finally, the dispersions were placed statically to observe its re-aggregation behavior. Fig. 1(a) shows the colloidal dispersion for HCNFs/water and HCNFs/DMF after ultrasonication at different time intervals. As seen in Fig. 1(a), the HCNFs/DMF dispersion was more stable, showing no signs of

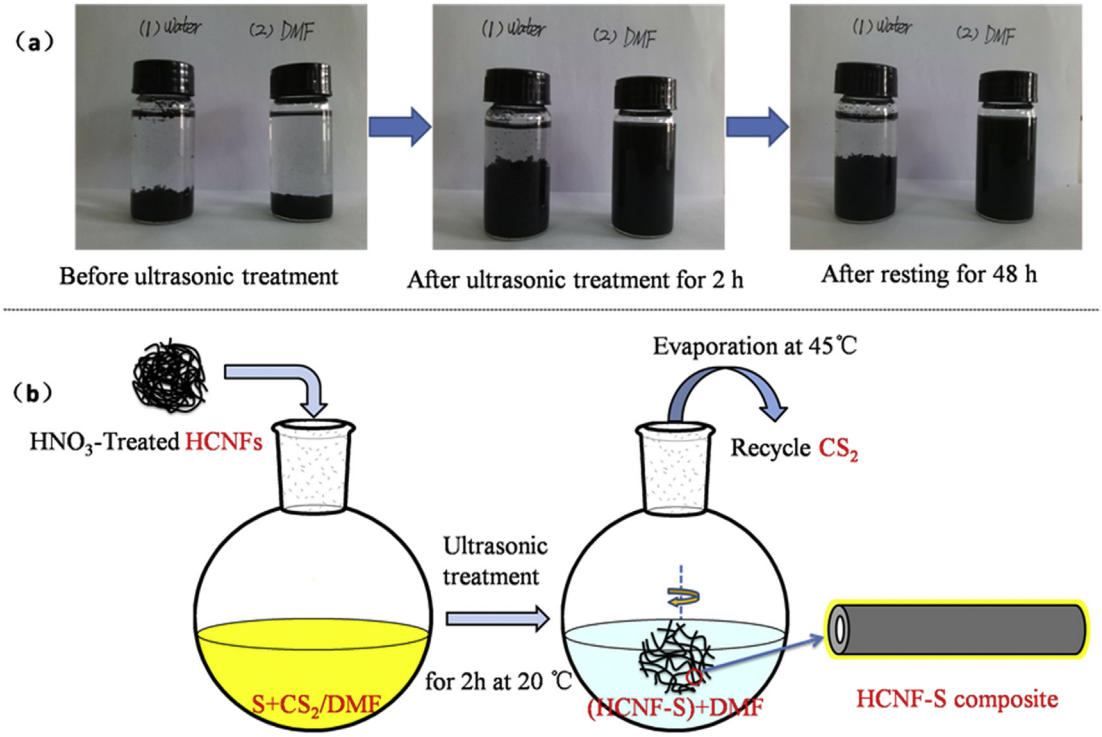

Fig. 1. (a) Images of HCNFs dispersion experiment. (b) Schematic of synthesis process for HCNF-S composite.

agglomeration even after 2 days. These observations are consistent with previous work [34]. Therefore, HCNF-sulfur composites were prepared by a mixed-solvent (DMF/CS_2) process in an organic solution. HCNFs were purchased from Sigma–Aldrich, and were soaked with concentrated nitric acid (HNO_3) at room temperature for 48 h before used. 1.0 g sublimed sulfur (Sigma–Aldrich, 100-mesh particle size powder) was first added into a flask filled with 20 ml N,N-Dimethylformamide (DMF, Aladdin reagent, AR) and 50 ml carbon disulfide (CS_2, Aladdin reagent, AR) to form a sulfur-containing DMF/CS_2 organic solution. 0.65 g HCNFs were then dispersed in the organic solution and ultrasonic treated at 20 °C for 2 h to achieve a homogenous suspension. Subsequently, the suspension was heated to 45 °C and stirred constantly for 12 h to evaporate CS_2 from the reaction mixture, during which sulfur recrystallized and formed HCNF-S composites. After cooling to the room temperature, the resulting suspension was filtered, and the precipitate was rinsed with ethyl alcohol several times to eliminate the residual DMF, then dried in a vacuum oven at 60 °C for 24 h. The schematic of the preparation process is shown in Fig. 1(b).

2.2. Material characterization

The morphology of the samples was investigated by field emission scanning electron microscopy (SEM, Nova Nano SEM 230) and transmission electron microscopy (TEM, Tecnai G2 20ST). The elements on the surface of sample were identified by energy-dispersive X-ray spectroscopy (EDS) and scanning transmission electron microscopy (STEM, Tecnai G2 F20)/energy dispersive X-ray spectroscopy (EDX). Powder X-ray diffraction (XRD, Rigaku3014) using Cu-K_α radiation was employed to identify the crystalline phase of HCNFs and the prepared HCNF-S composite. Thermogravimetric analysis (TGA, SDTQ600) was conducted in determining the sulfur content in the composite under N_2 atmosphere at a heating rate of 10 °C min^{-1}.

2.3. Electrochemical measurements

The working electrodes were prepared by a slurry coating procedure. The composite cathode slurry consisted of 80 wt% HCNF-S

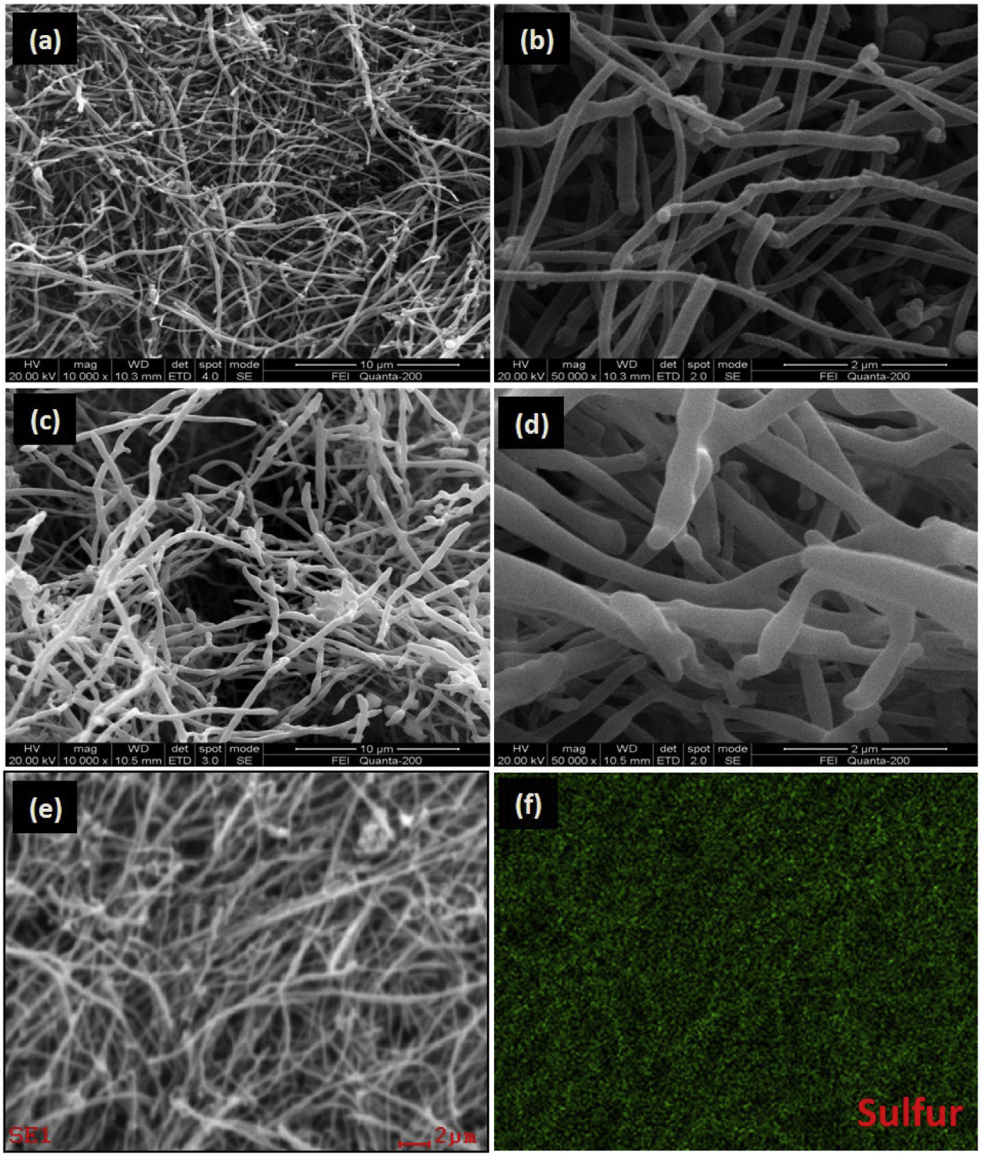

Fig. 2. SEM images of (a) and (b) HCNFs, (c) and (d) HCNF-S composite. EDS mapping of (e) and (f) HCNF-S composite revealing the distribution of sulfur.

composite, 10 wt% acetylene black and 10 wt% polyvinylidene fluoride (PVDF) dissolved in N-methyl pyrrolidinone (NMP). The slurry of the cathode was pressed onto a sheet of aluminum foil, dried at 60 °C overnight, then the cathode were cut into pellets with a diameter of 1.0 cm and dried for 12 h in a vacuum oven at 60 °C. CR2025-type coin cells were assembled in an argon-filled glove box to avoid contamination by moisture and oxygen. The electrolyte used was 1 M bis(trifluoromethane) sulfonamide lithium salt (LiTFSI, Sigma Aldrich) in a mixed solvent of 1,3-dioxolane (DOL, Acros Organics) and 1,2-dimethoxyethane (DME, Acros Organics) with a volume ratio of 1: 1, including 0.1 M $LiNO_3$ as an electrolyte additive. Lithium metal was used as counter electrode and reference electrode and celgard-2400 was used as separator. Specific capacity was corrected based on the mass of sulfur, and the typical sulfur mass loading on the electrode was about 1.5 mg cm^{-2}. Cyclic voltammetry (CV) and electrochemical impedance spectroscopy (EIS) measurements were conducted using PARSTAT 2273 electrochemical measurement system. CV tests were performed at a scan rate of 0.2 mV s^{-1} in the voltage range of 1.5 V–3.0 V. EIS measurements were carried out at open-circuit potential (OCP) in the frequency range between 100 kHz and 10 mHz with a perturbation amplitude of 5 mV. Galvanostatic charge/discharge tests were performed in the potential range of 1.5 V–3.0 V at 25 °C by using a LAND CT2001A battery-testing instrument.

3. Results and discussion

Fig. 2 shows the SEM morphological characterization of the HCNFs and the HCNF-S composite. TEM images of HCNF and HCNF-S composite and EDX/STEM of HCNF-S composite are shown in Fig. 3. It can be seen from Figs. 2(a) and (b) and 3(a) that the diameter of the HCNF is about 100 nm with a hollow structure. While sulfur is precipitating from the organic solution, HCNFs can serve as the support and sulfur deposits on HCNFs surface and grows up to wrap the whole HCNFs, as shown in Fig. 2(c) and (d), this is also reported in previous CNF–S study [31,35]. From Figs. 2(c) and (d) and 3(b), we can see that there is no distinct morphological difference between HCNF and the HCNF-S composite except for the dimension, suggesting a homogeneous distribution of sulfur in the HCNFs network and a uniform sulfur coating on the surface of the HCNFs [31,35,36]. Comparing with the TEM image of pure HCNF, the HCNF-S nanofiber exhibits a diameter of approximately 130 nm, a thin layer as marked by yellow arrows in Fig. 3(b) with a mean thickness of about 15 nm (the uncoated HCNF has a diameter of 100 nm) wrapping on the outer surface of HCNF (as seen inset in Fig. 3(b)) is discernible for the composite nanofiber, which can be identified as sulfur deposited on HCNFs. Further evidence of sulfur's existence in the HCNF-S composite is provided by scanning transmission electron microscopy (STEM). The HCNF-S composite of a single fiber with hollow structure is selected to test the distribution of sulfur across the nanofiber by EDX/STEM. As shown in Fig. 3(c) and (d), after fitting by a two-error function algorithm, carbon profile exhibits a valley/decrease in the middle and sulfur shows a similar tendency with enhanced peaks on the side, suggesting that sulfur is mainly present on the edge of HCNF. The similar result analysis about sulfur existence can also be seen in the reported literature [18,37,38]. This core–shell structure of HCNF-S composite is beneficial for constructing a sturdy three-dimensional carbon network to accommodate the mechanical stresses induced by volume changes caused by the reaction of sulfur during the discharge/charge cycles [30,31,35]. To confirm the presence of sulfur, energy-dispersive X-ray spectroscopy (EDS) mapping is performed on the whole carbon HCNF-S composite, elemental

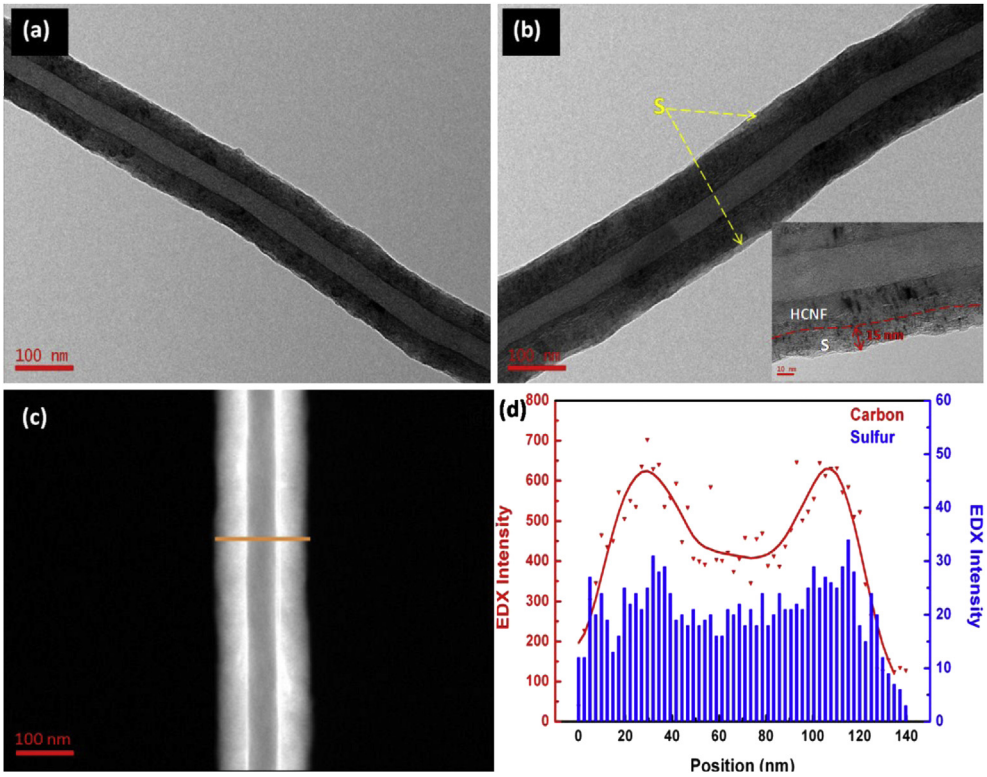

Fig. 3. TEM images of (a) HCNF and (b) HCNF-S composite (inset is a high-resolution image of an individual composite nanofiber). (c) Annular dark field (ADF)-STEM image of a HCNF coated with S and (d) EDX line profile across HCNF, showing the distribution of carbon and sulfur.

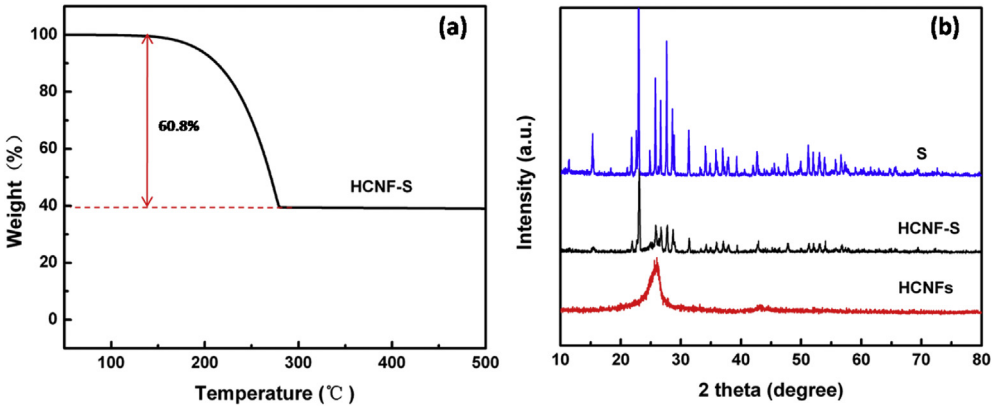

Fig. 4. (a) TGA curves of the HCNF-S composite. (b) XRD patterns of sulfur, HCNFs and HCNF-S composite.

sulfur are well distributed in the composite as shown in Fig. 2(e) and (f).

The sulfur content of the CNF-S composite is ascertained by thermogravimetric analysis (TGA), under a N_2 atmosphere, from room temperature to 500 °C at a heating rate of 5 °C min^{-1}. Fig. 4(a) shows the results obtained from TGA on the as prepared HCNF-S composite. It can be seen from Fig. 4(a) that the weight of the HCNF-S composite decreases with increasing temperature from 150 °C and the weight loss is continuous until the HCNF-S is heated to over 280 °C, which indicates that the reduction in weight of the HCNF-S composite is due to evaporation of sulfur. The sulfur content is 60.8 wt% in the HCNF-S composite.

The X-ray diffraction (XRD) patterns of elemental sulfur, HCNFs and HCNF-S composite are shown in Fig. 4(b). The XRD pattern of HCNFs shows a typical amorphous structure with one broad low-intensity peaks at around 26°, which can be ascribed to the (002) reflection of carbon. In Fig. 4(b), sulfur shows sharp diffraction peaks, which indicates high degree of crystalline, and diffraction angel of the highest peak with crystal plane of (222) is at 23.3°. Pure sulfur shows the typical reflection pattern of an orthorhombic type of sulfur (S_8, JCPDS#08 0247), which is stable at room temperature. In diffraction pattern of HCNF-S composite, the highest diffraction peak with low intensity appears at angel of 23.3° which corresponds to (222) crystal plane of sulfur [12]. The diffraction peak shows existence of sulfur crystal in HCNF-S composite. Compared with the pattern of sulfur, the XRD pattern of HCNF-S composite yields the broad diffraction peak around 26° and exhibits fewer peaks of sulfur with lower intensity. Our result is similar to several reported literature [3,26,39–42]. It may indicate that the sulfur is amorphous or some sulfur particles trapped in the hollow structure of HCNFs are unable to crystallize [40–42], which is in good agreement with the above SEM and TEM images. The results indicate that the mixed-solvent process method is effective in preparing HCNF-S composite.

Cyclic voltammogram (CV) curves of the HCNF-S composite cathode during the first three cycles are presented in Fig. 5(a). In the first cathodic scan, there are two remarkable reduction peaks at about 2.05 V and 2.35 V corresponding to the two discharge plateaus in Fig. 5(b). The peak at 2.35 V associates with the conversion of elemental sulfur to soluble lithium polysulfide (Li_2S_n, $4 \leq n \leq 8$); and the peak at 2.05 V is related to the reduction of lithium polysulfides to insoluble Li_2S_2 and Li_2S [43,44]. During the subsequent anodic scan process, only one sharp oxidation peak is observed in the potential of approximately 2.50 V–2.55 V, which corresponds to the conversion of Li_2S into high-order soluble polysulfides [45,46]. The higher oxidation potential in the CV is attributed to the polarization caused by the phase transition from insoluble Li_2S and Li_2S_2 to elemental sulfur [28,47]. In the subsequent scans, the little change of the current and peak areas for the oxidation process implies a stable structure of HCNF-S composite. Fig. 5(b) shows the discharge/charge voltage profiles of the HCNF-S composite cathode. The typical discharge curves at 1 C (by weight of sulfur, 1C = 1675 mA g^{-1}) as seen in Fig. 5(b) show the typical two-plateau behavior of a Li–S cell, which is due to the two step reaction of S with Li during the discharge process as demonstrated in CV measurement. As shown in Fig. 5(b), the HCNF-S composite shows a good utilization of active material with an initial specific discharge capacity of 1090 mA h g^{-1} and maintains a reversible capacity of

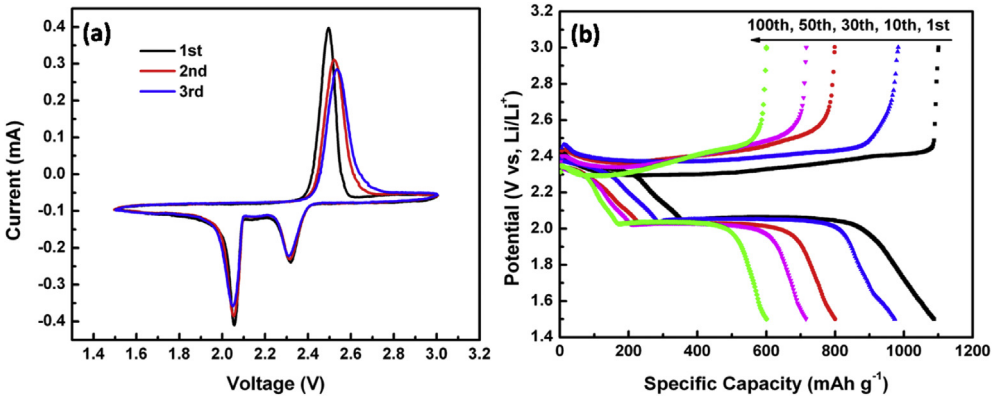

Fig. 5. (a) CV curves of the HCNF-S composite cathode at 0.2 mV s^{-1}. (b) Discharge/charge curves of HCNF-S composite cathode at 1 C.

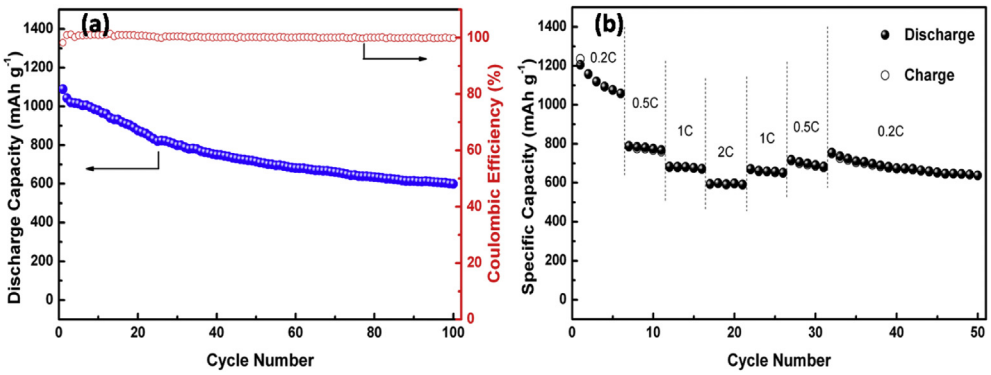

Fig. 6. (a) Cycling performance and coulombic efficiency of the HCNF-S composite cathode at 1C. (b) Rate performance of the HCNF-S composite cathode.

600 mA h g^{-1} after 100 cycles at a rate of 1 C. These indicate that the network structure of HCNFs is quite effective in suppressing the dissolution of polysulfides into the electrolyte and in maintaining high utilization of the active sulfur during the discharge/charge process.

Cyclic discharge capacity and coulombic efficiency of HCNF-S composite cathode at a high rate of 1 C between 3.0 V and 1.5 V at room temperature are shown in Fig. 6(a). It can be seen that the cell with HCNF-S composite cathode shows an initial specific discharge capacity of 1090 mAh g^{-1} and keeps a retention rate of 55% after 100 charge/discharge cycles, revealing higher capacities and better cycling stability than that of CNF-S composite reported before [31,36]. The good cycling performance is attributed to the structure of HCNF-S composite. Sulfur particles disperse well in the composite after homogeneous precipitation in DMF, which increases electric conductivity of sulfur. And the hollow structure and three-dimensional network structure with regular pores of HCNFs benefit the liquid electrolyte penetrating the composite and inhibit the loss of sulfur into the liquid electrolyte [31,35]. Besides, the cell also shows high coulombic efficiencies of around 100%, which indicates that self-discharge reaction between dissolved Li_2S_n and lithium anode and the shuttle effect are not apparent [30]. The combination of the HCNFs materials and composite cathode structure can achieve a high specific capacity sulfur cathode with stable cycling performance and high coulombic efficiency.

The rate capability of the HCNF-S composite cathode was then evaluated by cycling the cells at elevated charge/discharge rates up to 2 C. The reversible capacities at varying rates are plotted in Fig. 6(b). During the first 6 cycles, the discharge capacity faded gradually at 0.2 C rate and remained a capacity of 1058 mAh g^{-1}. A capacity of 780 mAh g^{-1} can be delivered at a higher rate of 0.5 C. Further increasing the charge/discharge rate to 1 and 2 C, a reversible capacity of 650 mAh g^{-1} (54% of its initial capacity) and 580 mAh g^{-1} (48% of its initial capacity) is reached, respectively. The cell also demonstrates excellent stability at each rate between 0.5 and 2 C. When the charge/discharge rate is back to 0.2 C after being continuously cycled at high rates for 25 times, a reversible capacity of 660 mAh g^{-1} can be restored, suggesting excellent redox stability of the HCNF-S composite. The excellent rate capability can be owing to the hollow structure of HCNFs and the good robustness and stability of the HCNF-S composite cathode material [48].

Electrochemical impedance spectra of HCNF-S composite at its OCP before cycling and after the cell completes the 50nd and 100th charges and equivalent circuit are shown in Fig. 7(a) and (b), respectively. It can be seen from Fig. 7(a) that the Nyquist plots of the HCNF-S electrode before discharge is composed of a semicircle at high frequency and medium frequency and an inclined line in the low frequency region. The high-frequency intercept on the real axis represents the ohmic resistance (Ro) of the cell, including the electrolyte and electrode resistances. The semicircle at high frequency to medium is attributable to the interface charge-transfer resistance (Rct), and the inclined line at the low-frequency region corresponds to Warburg impedance (Wo) [49–51]. After 50 and 100 cycles, the impedance responses of HCNF-S composite cathode have changed that two obvious semicircles appear, as shown in Fig. 7(a). The additional semicircle in the high frequency region can be explained as Li^+ migration through the SEI films (Rs) [3,52–55]. It can be seen from the Fig. 7(b) that the Nyquist plots are fitted by an equivalent circuit composed of Ro in series to a parallel circuit element that branches into Rs and constant phase element (CPE1), followed by another parallel circuit element that branches into Rct with Wo and the constant phase element (CPE2). Our results are similar to the reported literature [51–55]. The fitted Ro, Rs and Rct values obtained from the equivalent circuit are shown in inset of Fig. 7(a). The Ro value shows no obvious increase during 100 cycles. It indicates that the content of poorly conductive polysulfide dissolved in the electrolyte does not increase obviously during this cycle process [56,57]. The semicircle at high frequency is related to

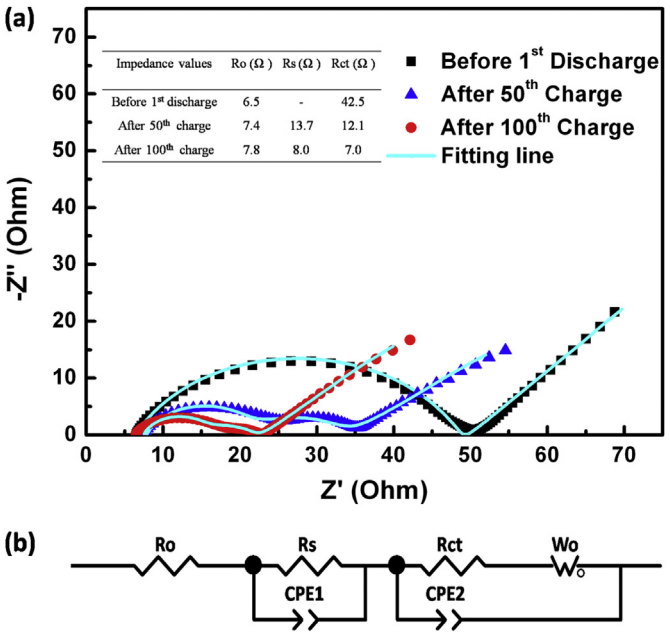

Fig. 7. (a) Nyquist plots and (b) the equivalent circuit of the prepared HCNF-S composite cathode before and after cycles. Inset (a) is resistance obtained from the equivalent circuit fitting of experimental date.

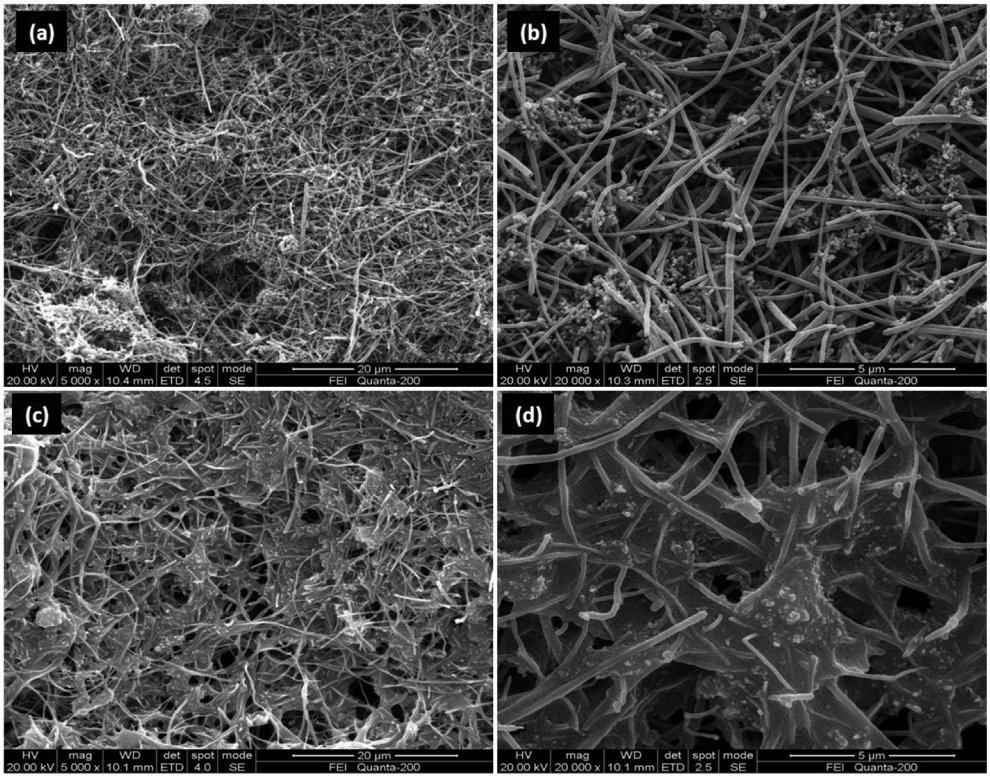

Fig. 8. SEM images of cathode (a and b) the as-prepared HCNF-S composite cathode and (c and d) HCNF-S composite cathode after 100 cycles.

the resistance and capacitance (a parallel connection of Rs and CPE1) of solid–state interface layers on the surfaces of the electrodes, which keeps decreasing during the cycles, this is possibly due to the reorganization of the passivation film and redistribution of the active material [58]; and the semicircle at medium frequency is related to the charge-transfer resistance and its related double-layer capacitance (parallel connection of Rct and CPE2), which shows a descending trend, indicating the continuous immersion of the electrolyte increases the reactive contact area [59] and implying the improved electrochemical environment for reaction within the cell. Furthermore, the intertwined carbon nanofibers could act as a continuous 3D network, which could provide efficient accessibility of active material to the electrolyte. The EIS results can also explain why the HCNF-S composite displays an excellent electrochemical performance.

To get further insight into the excellent electrochemical performance of HCNF-S composite cathode, the morphologies of the HCNF-S composite cathode before and after 100 cycles at 1 C rate are characterized. As shown in Fig. 8, the composite shows intertwined structure and inter-particulate porosity in the original HCNF-S composite electrode (Fig. 8(a) and (b)). The randomly intertwined HCNFs in the composite cathode construct a highly conductive network that facilitates fast transport of electrons within the entire cathode, while the ultrathin sulfur layer with a thickness of about 15 nm on the HCNFs enormously shortens the diffusion length of Li ions [31]. Moreover, the porous structure of the HCNF-S composite cathode enables easy infiltration of the electrolytes into the cathode and guarantees thorough exposure of sulfur-coating layers to Li ions in the electrolytes [35,36]. Therefore, good rate capability can be achieved for the HCNF-S composite cathode. The HCNF-S composite cathode keeps good porous structure, and no fracture occurs after long-time charge/discharge cycles, revealing good toughness of the composite cathode (Fig. 8(c) and (d)). This observation demonstrates that the porosity and interconnected network structure of hollow fibrous materials are helpful for anchoring sulfur and inhibiting polysulfide dissolving into the electrolyte [48], which contributes to the excellent electrochemical performance of the HCNF-S composite.

4. Conclusion

A hollow carbon nanofiber-sulfur composite, prepared by a simple method via a mixed-solvent process, exhibits perfect cycling stability as the cathode for Li–S batteries. An initial specific discharge capacity of 1090 mAh g^{-1} and a retention rate of 55% after 100 charge/discharge cycles at a high rate of 1 C is achieved. The results show that the highly conductive network-like HCNFs matrix allows fast electron conduction, provides a hollow and porous intertwined structure to anchor sulfur and absorb polysulfides, and suppresses the formation of residual Li_2S layer. The hollow fibrous HCNFs would be a promising carbon matrix for Li–S batteries and the simple synthetic method is expected to be practically applicable for high-performance Li–S batteries as the next-generation energy storage systems.

Acknowledgments

The authors thank the financial support of the Strategic Emerging Industries Program of Shenzhen, China (JCYJ201206 18164543322) and the Teacher Research Fund of Central South University (2013JSJJ027). We also thank the support of the Engineering Research Center of Advanced Battery Materials, the Ministry of Education, China.

References

[1] J. Nelson, S. Misra, Y. Yang, A. Jackson, Y. Liu, H. Wang, H. Dai, J.C. Andrews, Y. Cui, M.F. Toney, J. Am. Chem. Soc. 134 (2012) 6337–6343.

[2] X. Ji, K.T. Lee, L.F. Nazar, Nat. Mater. 8 (2009) 500–506.
[3] Y.X. Wang, S.L. Chou, H.K. Liu, S.X. Dou, J. Power Sources 244 (2013) 240–245.
[4] S.S. Zhang, J. Power Sources 231 (2013) 153–162.
[5] X. Liang, Y. Liu, Z. Wen, L. Huang, X. Wang, H. Zhang, J. Power Sources 196 (2011) 6951–6955.
[6] F. Wu, J. Chen, L. Li, T. Zhao, R. Chen, J. Phys. Chem. C. 115 (2011) 24411–24417.
[7] N. Jayaprakash, J. Shen, S.S. Moganty, A. Corona, L.A. Archer, Angew. Chem. Int. Ed. 50 (2011) 1–6.
[8] L. Yin, J. Wang, F. Lin, J. Yang, Y. Nuli, Energy Environ. Sci. 5 (2012) 6966–6972.
[9] W. Wei, J. Wang, L. Zhou, J. Yang, B. Schumann, Y. NuLi, Electrochem. Commun. 13 (2011) 399–402.
[10] G. He, X. Ji, L. Nazar, Energy Environ. Sci. 4 (2011) 2878–2883.
[11] Y.S. Su, A. Manthiram, Electrochim. Acta 77 (2012) 272–278.
[12] W. Ahn, K.B. Kim, K.N. Jung, K.H. Shin, C.S. Jin, J. Power Sources 202 (2012) 394–399.
[13] C. Zhang, H.B. Wu, C. Yuan, Z. Guo, X.W. Lou, Angew. Chem. Int. Ed. 51 (2012) 9592–9595.
[14] Y.S. Su, A. Manthiram, Chem. Commun. 48 (2012) 8817–8819.
[15] C. Liang, N.J. Dudney, J.Y. Howe, Chem. Mater. 21 (2009) 4724–4730.
[16] X. Li, Y. Cao, W. Qi, L.V. Saraf, J. Xiao, Z. Nie, J. Mietek, J.G. Zhang, B. Schwenzer, J. Liu, J. Mater. Chem. 21 (2011) 16603–16610.
[17] S.R. Chen, Y.P. Zhai, G.L. Xu, Y.X. Jiang, D.Y. Zhao, J.T. Li, L. Huang, S.G. Suna, Electrochim. Acta 56 (2011) 9549–9555.
[18] J. Guo, Y. Xu, C. Wang, Nano Lett. 11 (2011) 4288–4294.
[19] L. Yuan, H. Yuan, X. Qiu, L. Chen, W. Zhu, J. Power Sources 189 (2009) 1141–1146.
[20] C.S. Kim, A. Guerfi, P. Hovington, J. Trottier, C. Gagnon, F. Barray, A. Vijh, M. Armand, K. Zaghib, J. Power Sources 241 (2013) 554–559.
[21] F. Wu, J. Chen, R. Chen, S. Wu, L. Li, S. Chen, T. Zhao, J. Phys. Chem. C. 115 (2011) 6057–6063.
[22] L. Wang, X. He, J. Li, M. Chen, J. Gao, C. Jiang, Electrochim. Acta 72 (2012) 114–119.
[23] H. Zhao, Z. Peng, W. Wang, X. Chen, J. Fang, J. Xua, J. Power Sources 245 (2014) 529–536.
[24] J.Z. Wang, L. Lu, M. Choucair, J.A. Stride, X. Xu, H.K. Liu, J. Power Sources 196 (2011) 7030–7034.
[25] N. Brun, K. Sakaushi, L. Yu, L. Giebeler, J. Eckert, M.M. Titirici, Phys. Chem. Chem. Phys. 15 (2013) 6080–6087.
[26] C. Zhang, H.B. Wu, C. Yuan, Z. Guo, X.W. Lou, Angew. Chem. Int. Ed. 51 (2012) 1–5.
[27] L. Xiao, Y. Cao, J. Xiao, B. Schwenzer, M.H. Engelhard, L.V. Saraf, Z. Nie, G.J. Exarhos, J. Liu, Adv. Mater. 24 (2012) 1176–1181.
[28] C. Wang, W. Wan, J.T. Chen, H.H. Zhou, X.X. Zhang, L.X. Yuan, Y.H. Huang, J. Mater. Chem. A 1 (2013) 1716–1723.
[29] M. Rao, X. Song, E.J. Cairns, J. Power Sources 205 (2012) 474–478.
[30] G. Zheng, Y. Yang, J.J. Cha, S.S. Hong, Y. Cui, Nano Lett. 11 (2011) 4462–4467.
[31] M. Rao, X. Song, H. Liao, E.J. Cairns, Electrochim. Acta 65 (2012) 228–233.
[32] J.B. Xu, T.S. Zhao, J. Power Sources 195 (2010) 1071–1075.
[33] H.T. Ham, Y.S. Choi, I.J. Chung, J. Colloid Interface Sci. 286 (2005) 216–223.
[34] F. Inam, H. Yan, M.J. Reece, T. Peijs, Nanotechnology 19 (2008) 195710–195714.
[35] M. Rao, X. Geng, X. Li, S. Hu, W. Li, J. Power Sources 212 (2012) 179–185.
[36] Z. Deng, Z. Zhang, Y. Laia, J. Liu, Y. Liu, J. Li, Solid State Ionics 238 (2013) 44–49.
[37] M. Xiao, M. Huang, S.S. Zeng, D.M. Han, S.J. Wang, L.Y. Sun, Y.Z. Meng, RSC Adv. 3 (2013) 4914–4916.
[38] H.W. Chen, W.L. Dong, J. Ge, C.H. Wang, X.D. Wu, W. Lu, L.W. Chen, Sci. Rep. 3 (2013) 1910.
[39] F. Wu, J. Chen, L. Li, T. Zhao, Z. Liu, R. Chen, ChemSusChem. 6 (2013) 1438–1444.
[40] Y. Fu, Y.S. Su, A. Manthiram, ACS Appl. Mater. Interfaces 4 (2012) 6046–6052.
[41] Y.H. Qu, Z.A. Zhang, X.W. Wang, Y.Q. Lai, Y.X. Liu, J. Li, J. Mater. Chem. A 1 (2013) 14306–14310.
[42] K. Zhang, Q. Zhao, Z.L. Tao, J. Chen, Nano Res. 6 (2013) 38–46.
[43] Y. Jung, S. Kim, Electrochem. Commun. 9 (2007) 249–254.
[44] Y.J. Li, H. Zhan, S.Q. Liu, K.L. Huang, Y.H. Zhou, J. Power Sources 195 (2010) 2945–2949.
[45] X.Y. Tao, X.R. Chen, J. Mater. Chem. A 1 (2013) 3295–3301.
[46] J.C. Guo, Z.C. Yang, Y.C. Yu, H.D. Abrun, L.A. Archer, J. Am. Chem. Soc. 135 (2013) 763–767.
[47] J.W. Choi, G. Cheruvally, D.S. Kim, J.H. Ahn, K.W. Kim, H.J. Ahn, J. Power Sources 183 (2008) 441–445.
[48] K. Jin, X. Zhou, L. Zhang, X. Xin, G. Wang, Z. Liu, J. Phys. Chem. C 117 (2013) 21112–21119.
[49] Y.J. Choi, Y.D. Chung, C.Y. Baek, K.W. Kim, H.J. Ahn, J.H. Ahn, J. Power Sources 184 (2008) 548–552.
[50] V.S. Kolosnitsyn, E.V. Kuz'mina, E.V. Karaseva, S.E. Mochalov, Russ. J. Electrochem. 47 (2011) 793–798.
[51] Q.W. Tang, Z.Q. Shan, L. Wang, X. Qin, K.L. Zhu, J.H. Tian, X.S. Liu, J. Power Sources 246 (2014) 253–259.
[52] X.Y. Zhou, J. Xie, J. Yang, Y.L. Zou, J.J. Tang, S.C. Wang, L.L. Ma, Q.C. Liao, J. Power Sources 243 (2013) 993–1000.
[53] C. Zu, Y.S. Su, Y. Fu, A. Manthiram, Phys. Chem. Chem. Phys. 15 (2013) 2291–2297.
[54] M.S. Park, J.S. Yu, K.J.K.G. Jeong, J.H. Kim, T. Yim, Y.N. Jo, U. Hwang, S. Kang, T. Woo, H. Kim, Y.J. Kim, RSC Adv. 3 (2013) 11774–11781.
[55] V.S. Kolosnitsyn, E.V. Kuzmina, E.V. Karaseva, S.E. Mochalov, J. Power Sources 196 (2011) 1478–1482.
[56] C. Zu, Y. Fu, A. Manthiram, J. Mater. Chem. A 1 (2013) 10362–10367.
[57] L. Yuan, X. Qiu, L. Chen, W. Zhu, J. Power Sources 189 (2009) 127–132.
[58] Z.F. Deng, Z.A. Zhang, Y.Q. Lai, J. Liu, J. Li, Y.X. Liu, J. Electrochem Soc. 160 (2013) A553–A558.
[59] L. Xiao, Y. Cao, J. Xiao, B. Schwenzer, M.H. Engelhard, L.V. Saraf, Z. Nie, G.J. Exarhos, J. Liu, J. Mater. Chem. A 1 (2013) 9517–9526.